Current Biology 19, 267–276, February 24, 2009 ©2009 Elsevier Ltd All rights reserved DOI 10.1016/j.cub.2008.12.048

Article

A Novel Dynamin-Related Protein Has Been Recruited for Apicoplast Fission in *Toxoplasma gondii*

Giel G. van Dooren,[1] Sarah B. Reiff,[2] Cveta Tomova,[3] Markus Meissner,[4] Bruno M. Humbel,[3] and Boris Striepen[1,2,*]
[1]Center for Tropical and Emerging Global Diseases
[2]Department of Cellular Biology
University of Georgia
Athens, GA 30602
USA
[3]Electron Microscopy and Structural Analysis
Department of Biology, Faculty of Sciences
Utrecht University
3584 CH Utrecht
The Netherlands
[4]Department of Parasitology
Hygiene Institute
Heidelberg University School of Medicine
69120 Heidelberg
Germany

Summary

Background: Apicomplexan parasites cause numerous important human diseases, including malaria and toxoplasmosis. Apicomplexa belong to the Alveolata, a group that also includes ciliates and dinoflagellates. Apicomplexa retain a plastid organelle (the apicoplast) that was derived from an endosymbiotic relationship between the alveolate ancestor and a red alga. Apicoplasts are essential for parasite growth and must correctly divide and segregate into daughter cells upon cytokinesis. Apicoplast division depends on association with the mitotic spindle, although little is known about the molecular machinery involved in this process. Apicoplasts lack the conserved machinery that divides chloroplasts in plants and red algae, suggesting that these mechanisms are unique.
Results: Here, we demonstrate that a dynamin-related protein in *Toxoplasma gondii* (*Tg*DrpA) localizes to punctate regions on the apicoplast surface. We generate a conditional dominant-negative *Tg*DrpA cell line to disrupt *Tg*DrpA functions and demonstrate that *Tg*DrpA is essential for parasite growth and apicoplast biogenesis. Fluorescence recovery after photobleaching and time-lapse imaging studies provide evidence for a direct role for *Tg*DrpA in apicoplast fission.
Conclusions: Our data suggest that DrpA was likely recruited from the alveolate ancestor to function in fission of the symbiont and ultimately replaced the conserved division machinery of that symbiont.

Introduction

Plastid organelles trace their evolutionary origins to cyanobacteria that were incorporated into eukaryotic cells by a process of endosymbiosis. This evolutionary history dictates that they cannot be formed de novo. Instead, existing plastids divide to give rise to daughter organelles that partition into daughter cells upon cell division. Previously studied plastids contain an FtsZ-based division apparatus retained from the cyanobacterial endosymbiont [1]. In addition, plant and red algal plastid division involves a dynamin-like protein called ARC5 (also known as DRP5B [2, 3]).

Apicoplasts, the nonphotosynthetic plastids of apicomplexan parasites, must correctly divide and segregate into daughter cells for parasites to remain viable [4]. Surprisingly, apicomplexan genomes lack homologs to both ARC5 and FtsZ [5], suggesting that apicoplast division is mechanistically different than that in previously studied plastids. One striking difference is the association of the apicoplast with the centrosomes of the mitotic spindle [6, 7]. This association is thought to ensure proper segregation during cytokinesis, parceling out apicoplasts to a highly variable number of daughter cells formed in the complex apicomplexan budding process [8]. Though centrosome association provides a unifying model for segregation, it remains unclear how apicoplast fission occurs. One model suggests that fission depends on force generated by daughter cell budding [6], whereas electron microscopic studies identify apparent plastid division rings [9, 10], suggesting that protein components may mediate fission.

Dynamins are large GTPase proteins that function in a range of contractile processes, including the scission of endocytic vesicles, cytokinesis, nuclear remodelling, and the fission of mitochondria, chloroplasts, and peroxisome organelles [11–13], and we were interested in whether dynamins had a role in apicoplast division. Apicomplexan genomes encode three dynamin-related proteins that are phylogenetically distinct from ARC5. In this study, we characterize dynamin-related protein A (DrpA) in the apicomplexan *T. gondii*. We demonstrate that *Tg*DrpA is required for apicoplast fission, and we present a detailed model for how *Tg*DrpA functions in this process.

Results

T. gondii Contains Three Dynamin-like Proteins that Are Phylogenetically Distinct from ARC5 Dynamins

By using previously characterized proteins from yeast, plants, and red algae, we performed homology searching for dynamin-related proteins in apicomplexan parasites. We examined the genomes of *T. gondii*, *Plasmodium vivax*, *P. falciparum*, *Theileria parva*, and *Cryptosporidium parvum*. In each organism, we identified two characteristic dynamin-related proteins. To ascertain the evolutionary history of these dynamins, we performed phylogenetic analyses on a multiple sequence alignment of a broad spectrum of dynamin-related proteins. These indicated that ARC5/Drp5B dynamins from plants, diatoms, green algae, and red algae cluster together with strong bootstrap support and are sisters to a group of dynamins involved in cytokinesis [12]. These ARC5 and related proteins are clearly distinct from apicomplexan dynamins (Figure 1). One apicomplexan dynamin group (that we term dynamin-related protein B, or DrpB) forms a well-supported clade that includes dynamins from ciliates, a phylum of alveolates related to Apicomplexa (Figure 1; [14] and [15], this issue of *Current Biology*).

*Correspondence: striepen@cb.uga.edu

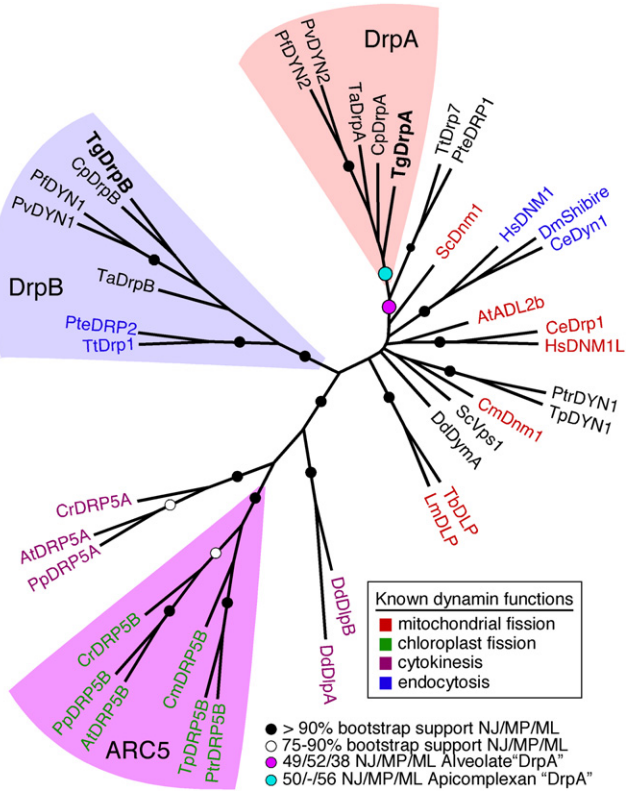

Figure 1. Phylogenetic Analyses of Dynamins

We generated a multiple sequence alignment of the conserved region of a range of dynamin-related proteins. The analysis included 449 residues and 39 taxa. We generated phylogenetic trees with PHYLIP, performing bootstrapping with 400 replicates. Bootstrap values based on neighbor joining (NJ), maximum parsimony (MP), and maximum likelihood (ML) analyses were determined. In this figure, we depict the consensus maximum likelihood tree.

Dynamin homologs included in the analysis are from *Drosophila melanogaster* (DmShibire); human (HsDNM1 and HsDNM1L); *Caenorhabditis elegans* (CeDyn1 and CeDrp1); *Cyanidioschyzon merolae* (CmDnm1 and CmDRP5B); *Dictyostelium discoideum* (DdDymA, DdDlpA, and DdDlpB); the diatoms *Thalassiosira pseudonana* (TpDYN1 and TpDRP5B) and *Phaeodactylum tricornutum* (PtrDYN1 and PtrDRP5B); *Saccharomyces cerevisiae* (ScVps1 and ScDnm1); *Arabidopsis thaliana* (AtADL2b, AtDRP5A, and AtDRP5B); *Physcomitrella patens* (PpDRP5A and PpDRP5B); *Chlamydomonas reinhardtii* (CrDRP5A and CrDRP5B); the ciliates *Tetrahymena thermophila* (TtDrp1 and TtDrp7) and *Paramecium tetraurelia* (PteDRP1 and PteDRP2); the apicomplexans *Plasmodium falciparum* (PfDYN2 and PfDYN1), *Plasmodium vivax* (PvDYN2 and PvDYN1), *Toxoplasma gondii* (TgDrpA and TgDrpB), *Theileria annulata* (TaDrpA and TaDrpB), and *Cryptosporidium parvum* (CpDrpA and CpDrpB); and the trypanosomatids *Trypanosoma brucei* (TbDLP) and *Leishmania mexicana* (LmDLP).

The other apicomplexan dynamin (which we term DrpA) forms a clade with ciliate dynamins that is not well supported by bootstrap analysis. Removing ARC5 and related sequences enables us to incorporate more characters in our analysis, and these additional data suggest that DrpA also forms an alveolate-specific clade (Figure S1A available online). A third protein with some similarity to dynamins is also present in apicomplexan genomes. These so-called DrpC proteins match only to the GTPase domain of dynamins, and phylogenetic analyses indicate that DrpCs are distinct from ARC5 dynamins (Figure S1B). We conclude that ARC5 is not a conserved component in apicoplast division.

*Tg*DrpA Localizes to the Periphery of the Apicoplast

To characterize the function of DrpA in *Toxoplasma gondii*, we examined its localization. We generated parasites expressing the entire open reading frame of *Tg*DrpA fused to an N-terminal HA tag, expressed from the native *Tg*DrpA promoter, and performed immunofluorescence assays. *Tg*DrpA localizes in many small patches throughout the cytosol of *T. gondii*, and a major component of *Tg*DrpA fluorescence clusters at the apical end of the cell (Figure 2A). Colocalization with the apicoplast stromal marker acyl carrier protein (ACP) indicates that this cluster occurs around the periphery of the apicoplast (Figure 2A). During division, apicoplasts form a distinctive U shape, with the base of the U being the point of organelle fission [6, 10]. In dividing apicoplasts, we typically observed *Tg*DrpA localizing to this point of fission, as well as to the ends of the organelle (Figures 2B and 2C, arrows). Later in apicoplast fission, when the base of the apicoplast becomes more constricted, the punctate dot of *Tg*DrpA observed early in the process appears as a more tubule-like structure between the dividing lobes of the apicoplast (Figure 2C, arrowheads). We found that *Tg*DrpA does not localize to the Golgi (Figure S2A) and only occasionally localizes to the mitochondrion (Figure S2B).

We performed an anti-HA western blot on proteins extracted from the HA-DrpA cell line. This revealed the presence of a band of ~90 kDa, conforming to the expected size of HA-tagged DrpA (Figure 2D). We next performed protease protection assays in conditions in which cytosolic, but not apicoplast stromal, markers were accessible to thermolysin. We found that *Tg*DrpA was sensitive to thermolysin (Figure S2C), consistent with *Tg*DrpA localizing to the cytosol. In the absence of clear markers for the four membranes that surround the apicoplast, our data cannot rule out the possibility that DrpA might localize to one or more of these intermembrane spaces.

*Tg*DrpA Is Essential for Parasite Growth

Having established the localization of *Tg*DrpA, we next wanted to determine its function. Dynamin proteins are self-assembling GTPases that contain an N-terminal GTPase domain, a middle domain, and a C-terminal GTPase effector domain (GED) (Figure 3A, top). Expression of dynamins with mutations in the GTP-binding site has been shown in other systems to specifically disrupt dynamin function in a dominant-negative fashion (e.g., [16, 17]). We generated a dominant-negative DrpA in which a lysine in the GTP-binding site was changed to an alanine (DrpA^{K42A}). To generate stable cell lines inducibly expressing dominant-negative DrpA, we fused a destabilization domain (DD) tag to the N terminus of DrpA^{K42A} (Figure 3A, bottom). DD tagging promotes proteosomal degradation of the protein, with degradation prevented by the small molecule Shield-1 [18, 19]. To determine whether we could regulate expression of DD-DrpA^{K42A}, we grew parasites for 0 to 20 hr on 0.1 μM Shield-1, extracted proteins, and performed western blotting. In the absence of Shield-1, we detected low levels of DD-DrpA^{K42A} (Figure 3B). Levels increased 3 hr after the addition of Shield-1 and were maximal after about 9 hr (Figure 3B).

To determine whether DrpA is essential for parasite growth, we expressed tandem yellow fluorescent protein (YFP) in DD-DrpA^{K42A} mutant parasites and monitored growth by using a fluorescence growth assay [20]. DD-DrpA^{K42A} mutant parasites grew robustly in the absence of Shield-1 (Figure 3C, bottom). However, compared to wild-type parasites (Figure 3C, top),

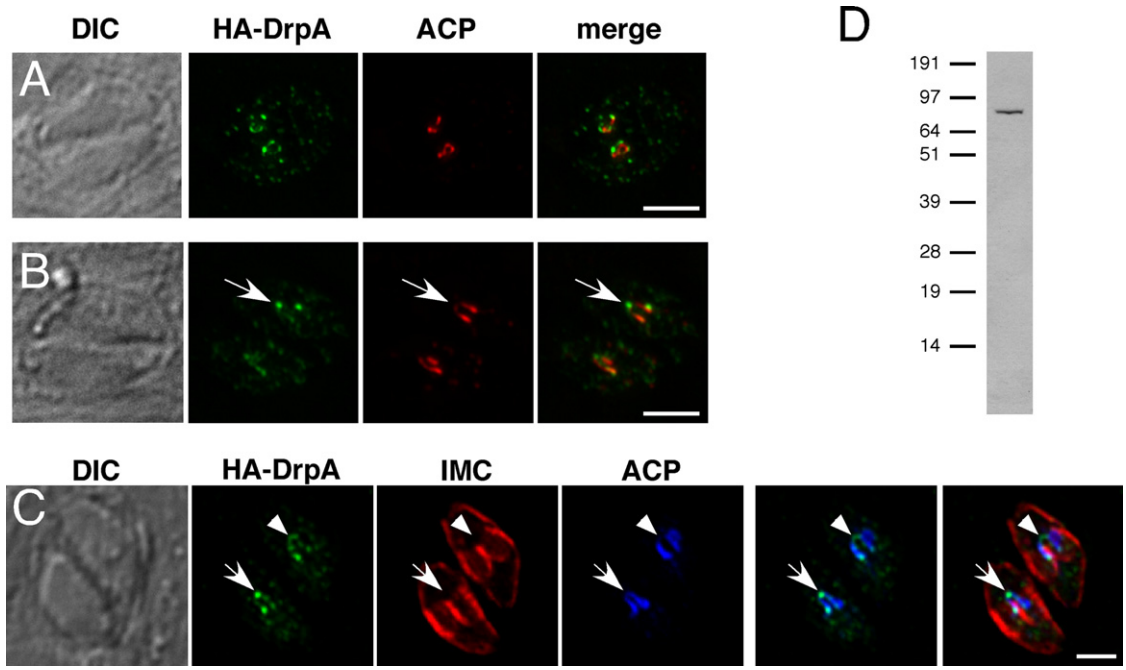

Figure 2. *Tg*DrpA Localizes to the Apicoplast

(A and B) Immunofluorescence assays of a cell line that expresses HA-tagged *Tg*DrpA, labeled with anti-HA (green) and the apicoplast stromal marker anti-acyl carrier protein (ACP; red) antibodies. Arrows point to sites of apicoplast fission. Scale bars, 2 μm.

(C) Immunofluorescence assay of the HA-*Tg*DrpA cell line, labeled with anti-HA (green), anti-IMC (red), and anti-ACP (blue) antibodies. Arrows point to sites of apicoplast fission, where HA-*Tg*DrpA forms a punctate dot. Arrowheads point to the tubule-like structure adopted by HA-*Tg*DrpA later in apicoplast fission when the apicoplast has become further constricted. Scale bar, 2 μm.

(D) Anti-HA western blot of the HA-*Tg*DrpA cell line, labeling a protein band at ~90 kDa.

growth of DD-DrpA^{K42A} parasites in 0.1 μm Shield-1 was slowed after about 5 days. Preincubation of DD-DrpA^{K42A} mutant parasites in Shield-1 for 3 days resulted in negligible growth of the parasites.

As a second measure for parasite growth, we performed plaque assays. In the presence of Shield-1, we saw a severe reduction in plaque size compared to the no Shield-1 control (Figure S3A), consistent with the importance of *Tg*DrpA for parasite growth. We also preincubated parasites for 12 hr in the presence of Shield-1, washed out the drug for an additional 12 hr, and set up plaque assays in fresh flasks in the absence or presence of Shield-1. As expected, parasites grown in the presence of Shield-1 exhibited severe defects in growth. Interestingly, cultures preincubated with Shield-1 for 12 hr and then grown in the absence of Shield-1 showed plaques of a similar size as parasites grown entirely in the absence of Shield-1, but the number of plaques was reduced by 63% when compared to the no Shield-1 control. This suggests that ~40% of parasites are no longer viable after a 12 hr incubation in Shield-1. We conclude that *Tg*DrpA is essential for parasite growth and that ablation of *Tg*DrpA function results in a delayed death effect that is typical of processes affecting the apicoplast [4, 21].

*Tg*DrpA Is Essential for Normal Apicoplast Morphology and Biogenesis

To directly test the impact of loss of DrpA function on the apicoplast, we generated a DD-DrpA^{K42A} mutant cell line that targeted red fluorescent protein (RFP) to the apicoplast. In the absence of Shield-1, apicoplast morphology appeared normal, with a single apicoplast organelle localizing to the apical end of each parasite (Figure 4A). Upon incubation in Shield-1, we observed severe defects in apicoplast biogenesis (Figures 4B–4D). Apicoplasts frequently occurred as branched tubules that appeared to connect several cells within a vacuole (Figures 4C and 4D). We also observed apicoplasts mislocalized to the basal end of parasites (Figure 4B) or entirely missing from one or more parasites within a vacuole (Figures 4C and 4D). To quantify these defects, we grew DD-DrpA^{K42A} mutant parasites for 0, 3, 6, 9, 12, and 20 hr in Shield-1. We imaged 100 four-cell vacuoles and scored apicoplast morphologies into four categories: normal apicoplasts (as in Figure 4A), basal stunted (Figure 4B), basal elongated (Figures 4C and 4D), and cells in which apicoplasts were absent (Figures 4C and 4D). In the absence of Shield-1, most apicoplasts appeared normal (Figure 4E). After 6 hr of growth on Shield-1, most apicoplasts localized to the basal end of the cell and were stunted in appearance. After around 12 hr, an increasing number of the basally localized apicoplasts were elongated, and ~40% of parasites had lost their apicoplast (Figure 4E). This value correlates to the loss of viability in ~40% of parasites after 12 hr incubation in Shield-1 (Figure S3A), and we hypothesize that the growth defects that we observe in the *Tg*DrpA^{K42A} mutant result from loss of this essential organelle.

To gain a dynamic understanding of the observed phenotypes, we performed time-lapse imaging of mutant parasites expressing cytosolic YFP and apicoplast-targeted RFP. We added Shield-1 to parasites 6 hr before commencing imaging. Initially, there were no obvious defects in apicoplast morphology, with both cells in the two-cell vacuole containing a single, apically localized apicoplast (Figure 4F and Movie S1). After ~150 min, apicoplasts from both cells formed a U shape, typical of apicoplasts immediately preceding fission [6, 10].

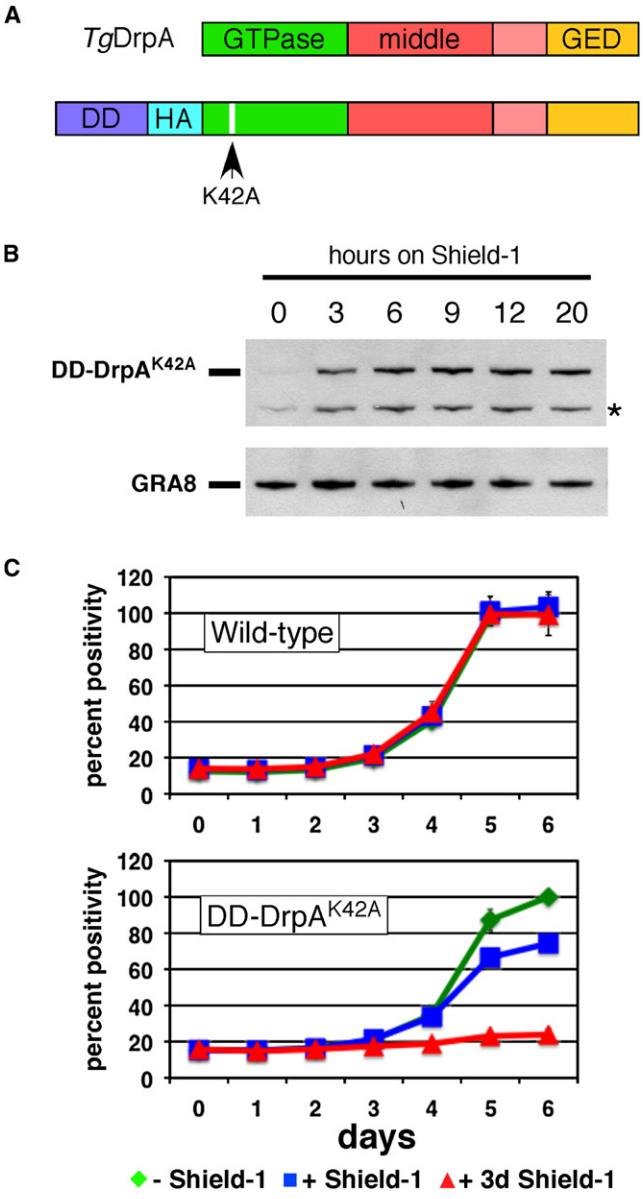

Figure 3. *Tg*DrpA Is Essential for Parasite Growth

(A) Dynamin-related proteins such as *Tg*DrpA consist of three conserved domains: an N-terminal GTPase domain, a middle domain, and a C-terminal GTPase effector domain (GED). To generate dominant-negative *Tg*DrpA mutants, we mutated the lysine in the GTP-binding motif of the GTPase domain to alanine (K42A). We fused an N-terminal destabilization domain (DD) and HA tag to this construct and generated clonal cell lines.

(B) To demonstrate regulated expression of DD-DrpA^{K42A}, we performed western blotting of cells grown for 0 to 20 hr in 0.1 μM Shield-1, probing blots with anti-HA antibodies and anti-GRA8 antibodies as a loading control. The asterisk represents a probable degradation product of DD-DrpA^{K42A}.

(C) We performed fluorescence growth assays on wild-type (top) and DD-DrpA^{K42A} (bottom) parasites expressing tandem-YFP. Parasites were grown in the absence of Shield-1 (green diamonds), in the presence of Shield-1 (blue squares), or preincubated for 3 days in the presence of Shield-1 before the assay, and they continued to grow in Shield-1 (red triangles). Error bars represent one standard deviation from the mean.

Subsequent imaging revealed that apicoplasts are unable to divide. Between ~20 and ~30 min later, cytokinesis commenced, with apicoplasts not dividing and becoming localized to the basal end of the cell (Figure 4F). We followed this vacuole for an additional 6 hr. Apicoplasts remained localized to the basal end of each cell in the vacuole, remaining in a small "stumpy" form. After about 5 hr, apicoplasts began elongating from the basal end of the cell. These data suggest that apicoplast morphology is normal up to the point of apicoplast division. Unable to divide, apicoplasts localize to the basal end of the cell and elongate before the next round of cell division.

We sought to quantify the basal localization of apicoplasts in the DD-DrpA^{K42A} mutant. We generated a DD-DrpA^{K42A} mutant cell line that expresses YFP-MORN1 and apicoplast RFP. MORN1 forms a contractile, basal complex in parasites (Figure 5A, arrowheads; [22, 23]), in addition to labeling the centrocone and growing daughter bud. In the presence of Shield-1, apicoplasts exit parasites through the YFP-MORN1-labeled basal complex (Figure 5B, arrowheads), with the apicoplast constricting at the basal complex (Figure 5B, inset). We grew parasites for 24 hr on Shield-1 and measured the distance between the basal complex and the apicoplast of the same cell. In the absence of Shield-1, the average distance of the apicoplast from the basal complex is 2.710 μm (SD, 0.546), whereas the value drops to 0.535 μm (SD, 0.672) in the presence of Shield-1 (Figure 5C). We next examined the DrpA mutant phenotype by electron microscopy. We observed apicoplasts localizing to the basal end of the parasite and, in some cases, exiting the parasite (Figures 5D and 5E, pink arrows).

We conclude that incubation of the DD-DrpA^{K42A} mutant in Shield-1 results in rapid and severe defects in apicoplast biogenesis and division. The DrpA^{K42A} mutant is predicted to act in a dominant-negative way to disrupt DrpA function. However, the data presented in Figures 4 and 5 do not rule out the possibility that the observed defects in apicoplast fission are a consequence of DrpA overexpression. To test this, we overexpressed wild-type DrpA, the DrpA^{K42A} mutant, and DrpA where the entire GTPase domain was deleted. We observed no effects on apicoplast biogenesis in cells that overexpress wild-type DrpA, whereas deletion of the entire GTPase domain resulted in apicoplast biogenesis defects identical to the DrpA^{K42A} point mutant (Figures S3B–S3F). We conclude that the DrpA^{K42A} mutant acts in a dominant-negative way to disrupt native *Tg*DrpA functions. We examined the effects of disrupting *Tg*DrpA function on other cellular functions. We found that DrpA has no role in protein targeting to the apicoplast or secretory pathways or in biogenesis of micronemes and rhoptries, specialized secretory organelles in Apicomplexa (Figures S4A–S4C). We found that, although there were no consistent defects, we could not entirely rule out a minor role for DrpA in mitochondrial biogenesis (Figures S4D and S4E).

*Tg*DrpA Mutants Are Incapable of Apicoplast Fission

Our data indicate that *Tg*DrpA is essential for apicoplast biogenesis. To elucidate the mechanism of *Tg*DrpA function in this process, we examined whether *Tg*DrpA has a role in apicoplast fission. In the absence of apicoplast fission, we predicted that apicoplasts from adjoining cells would remain connected. To experimentally test this, we performed fluorescence recovery after photobleaching (FRAP). We imaged DrpA^{K42A} parasites that express apicoplast-targeted RFP, grown in the absence or presence of Shield-1. We laser bleached apicoplast fluorescence from one parasite within a vacuole and measured recovery over 2 min. In the absence of Shield-1, we observed no fluorescence recovery of apicoplast fluorescence (Figures 6A and 6B and Movie S2). Average recovery in fluorescence after 2 min was 0.8% of relative fluorescence units, with

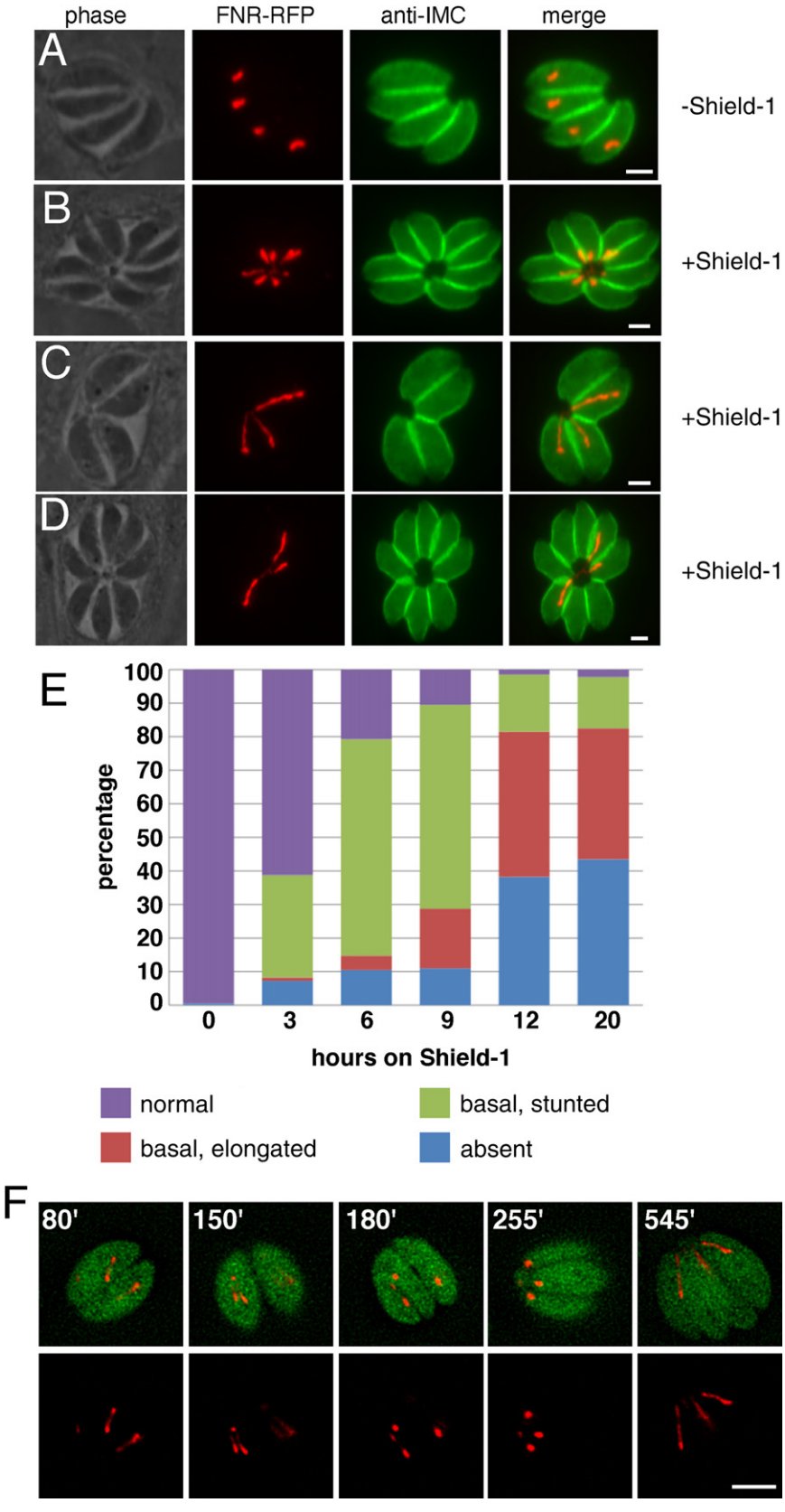

Figure 4. *Tg*DrpA Is Essential for Apicoplast Biogenesis

(A–D) Immunofluorescence assays of DD-DrpA^{K42A} parasites coexpressing apicoplast-targeted RFP (red), colabeled with anti-IMC antibodies (green). In the absence of Shield-1, every parasite contains a single apically localized apicoplast (A). In the presence of Shield-1, apicoplasts localize to the basal end of the parasite (B), frequently elongating toward the apical end of the cell and being absent in some cells (C and D). Scale bars, 2 μm.

(E) Quantification of the apicoplast defect in DD-DrpA^{K42A} parasites. We grew parasites for 0–20 hr on Shield-1 and imaged 100 four-cell parasite vacuoles. We classified apicoplasts into four categories: normal apicoplasts (purple), basal stunted apicoplasts (green), basal elongated apicoplasts (orange), and cells lacking apicoplasts (blue).

(F) Time-lapse imaging of apicoplasts in DD-DrpA^{K42A} parasites coexpressing cytosolic YFP and apicoplast-targeted RFP, grown in the presence of Shield-1. Scale bar, 2 μm.

a standard deviation of 0.9%. For parasites grown in Shield-1, we saw a consistent and significant recovery of fluorescence (Figures 6C and 6D and Movie S3). Average recovery in fluorescence after 2 min was 22.3%, with a standard deviation of 6.2%. Our data suggest that apicoplasts of adjoining cells in a single vacuole maintain a physical connection in the DrpA mutant, consistent with a defect in apicoplast fission. We performed similar FRAP analysis on mitochondrial fluorescence and found negligible recovery (Figures S4F–S4I).

Having established that *Tg*DrpA is required for apicoplast fission, we sought to elucidate the mechanistic role of *Tg*DrpA in this process. *T. gondii* daughter cells form within mother cells by internal budding (Figure 7A; [8]). The scaffold of the daughter buds consists of subpellicular microtubules and an inner membrane complex (IMC), flattened membrane sacs that are stabilized by a network of IMC proteins. Daughter buds form near the centrosomes and extend toward the basal end of the mother cell, incorporating the nucleus and various organelles before contracting at the base to enclose the newly formed daughter (Figure 7A; [23, 24]). MORN1 is a recently identified protein that localizes to a ring at the growing end of the daughter bud and ultimately forms the basal complex (Figure 7A; [8, 22, 23, 25]). In addition, MORN1 localizes to the centrocone, an elaboration of the nuclear envelope that contains the mitotic spindle and localizes adjacent to the centrosome. Immediately before apicoplast fission, the apicoplast typically adopts a U shape, with the ends of the daughter bud localizing to the base of the U (Figures 7B and 2C; [6]). We have previously hypothesized that the growing daughter bud functions in apicoplast division,

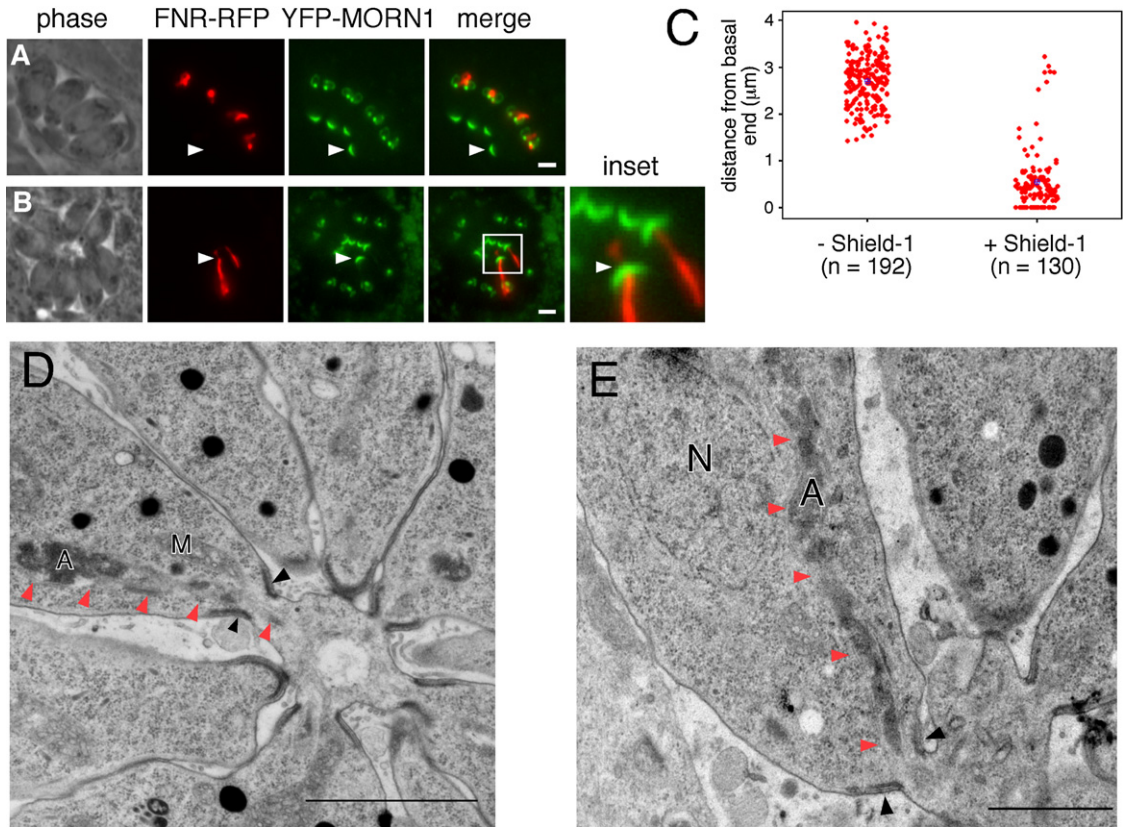

Figure 5. Apicoplasts Localize to the Basal End of Parasites upon Overexpression of Dominant-Negative *Tg*DrpA

(A and B) Live cell imaging of DD-DrpA^{K42A} parasites grown in the absence (A) or presence (B) of Shield-1, coexpressing FNR-RFP and YFP-MORN1. The arrow depicts the basal complex of a parasite, colocalizing in (B) with a point of constriction in the apicoplast (inset). Scale bars, 2 μm.

(C) Quantification of the distance between the YFP-MORN1-labeled basal complex and the nearest point of the apicoplast. DD-DrpA^{K42A} parasites were grown in the absence (left) or presence (right) of Shield-1, with distance in μm shown on the y axis. The blue circle represents the mean value for each data set.

(D and E) Electron micrograph images of DD-DrpA^{K42A} parasites grown on Shield-1. The basal end of parasites is marked by an electron dense area that likely corresponds to the contractile, MORN1-containing basal complex (black arrowheads). Apicoplasts (A) localize to the basal end of the parasites (pink arrowheads). The mitochondrion (M) and nucleus (N) are also shown. Scale bars, 1500 nm in (D) and 1000 nm in (E).

possibly generating the force necessary for fission [5, 6]. To examine this, we performed time-lapse imaging on the apicoplast RFP/DrpA^{K42A} mutant cell line grown in the absence of Shield-1 with YFP-MORN1 as a dynamic marker for the growth of the daughter bud (Figure 7D). After 35 min of imaging, each cell contains a single apicoplast and two MORN1 rings (Figure 7D and Movie S4). After 70 min, the MORN1 rings have moved toward the basal ends of the parasites. The apicoplast in the bottom parasite has adopted a U shape, with the two MORN1 rings localized at the base of the U. As daughter budding proceeds, the U shape of the apicoplast elongates, and, after 90 min, the MORN1 rings have moved further toward the basal end of the mother cell, and the apicoplast in this parasite has divided. After 100 min, the MORN1 ring has extended further still toward the basal end of the cell, and the apicoplasts remain at the apical end of the forming daughters associated with the centrosomes/centrocones. Soon after, the cells undergo cytokinesis, with the MORN1 rings becoming the basal complex of the newly formed daughter cells (Movie S4).

These data suggest that growth of the daughter bud is involved in generating the U-shaped apicoplast and that apicoplast division occurs when the MORN1 ring localizes to the base of the U. This raises two hypotheses for the role of DrpA in apicoplast fission: DrpA may function in formation of the daughter bud, which, in turn, is necessary for apicoplast fission, or DrpA functions directly in apicoplast fission and has no effect on daughter bud formation. To test this, we visualized the daughter bud of DrpA^{K42A} mutants coexpressing apicoplast RFP by immunofluorescence assays with an anti-IMC antibody, growing parasites in the presence of Shield-1. In parasites in which apicoplasts are unable to divide, the daughter bud appears normal (Figure 7C). To examine daughter bud formation and apicoplast fission in a more dynamic way, we performed time-lapse imaging on the previously described YFP-MORN1 and apicoplast-targeted RFP cell line grown in the presence of Shield-1 (Figure 7E). We examined a four-cell vacuole grown for 6 hr in Shield-1 wherein apicoplast morphology initially appeared normal. After 40 min, we see the development of MORN1 rings at the apical end of the parasites near the apicoplast (Figure 7E and Movie S5). After 90 min, we see the formation of U-shaped apicoplasts in each parasite, with the two MORN1 rings for each parasite localizing at the base of the U. Purple arrows indicate the direction of daughter cell budding. At 110 min, the U-shaped apicoplasts have stretched out

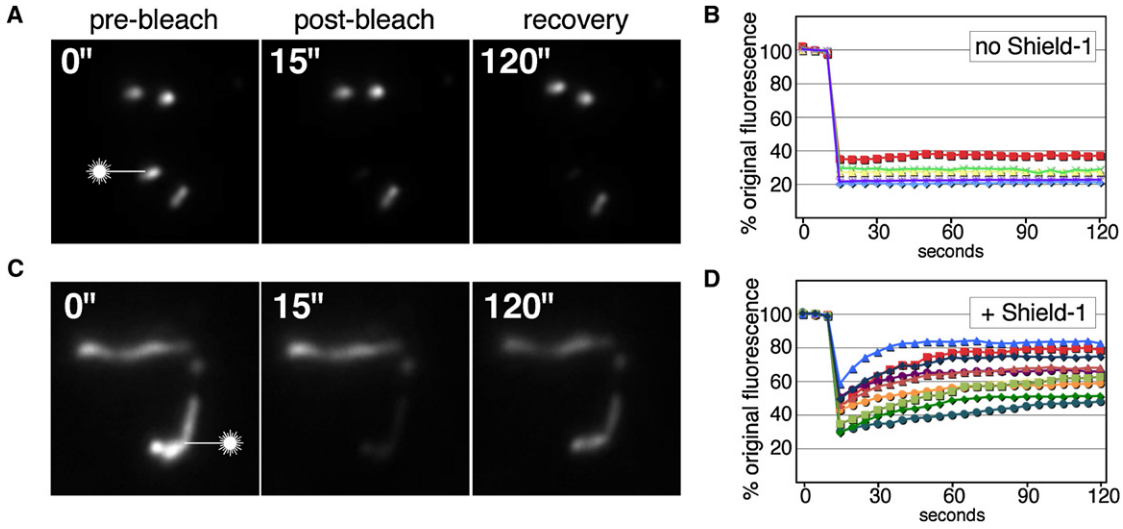

Figure 6. Disruption of *Tg*DrpA Function Results in Defects in Apicoplast Fission

(A–D) Fluorescence recovery after photobleaching in apicoplasts of DD-DrpA^{K42A} parasites grown in the presence or absence of Shield-1. We imaged parasites at 5 s intervals over 2 min, bleaching a diffraction-limited region of the field of view (at the position indicated by the laser symbol) after 10 s. (A) and (C) show images from single experiments, imaged before (left, 0"), directly after (middle, 15"), and at the end of the experiment (right, 120"). (B) and (D) show quantifications of fluorescence recovery over time in five (B) or ten (D) independent experiments. DD-DrpA^{K42A} parasites coexpressing apicoplast-targeted RFP were grown in the absence (A and B) or presence (C and D) of Shield-1.

further but have not divided. After 125 min, cytokinesis has begun. In the top cell, the MORN1 rings have contracted to close off the newly formed daughter cells (arrowheads), but the apicoplast is clearly not divided. The apicoplast ends remain attached to centrosomes/centrocones (white arrow). At 5 min later, one apicoplast branch has released from the centrosome/centrocone and appears to localize to the basal end of the daughter cell (white arrow). After 195 min of imaging, the apicoplasts of all eight newly formed daughters localize to the basal end of the cell and are no longer connected to the centrosomes. We conclude that, after ablation of DrpA function, daughter cell budding is normal. Furthermore, apicoplast division appears normal up to the point of organellar fission. Together with the localization of native DrpA to the base of the U-shaped apicoplast (Figures 2B and 2C), these data suggest a direct role for DrpA in apicoplast fission. Although daughter budding has a role in extension of the apicoplast into an elongated U shape [5, 6], this extension is not sufficient to mediate apicoplast fission.

Discussion

The data presented in this study indicate that *Tg*DrpA functions in apicoplast fission. Curiously, apicomplexan DrpA proteins are phylogenetically distinct from ARC5 dynamins that play a similar role in chloroplast division in plants [2]. This suggests that DrpA evolved from a host cytoplasmic dynamin that was recruited to endosymbiont division independently of ARC5, a remarkable example of convergent evolution. Dynamins appear to be promiscuous membrane-modifying enzymes, whose cellular function is largely dependent on the membranes to which they are recruited. It is, therefore, of considerable interest to identify the mechanisms of *Tg*DrpA recruitment to the apicoplast. The apicoplast progenitor was a red alga [26, 27] that likely had an ARC5 and FtsZ-based chloroplast division apparatus. Why was it necessary to evolve a second dynamin to replace the function of these ubiquitous plastid division proteins? A crucial step in the establishment of a successful endosymbiotic organelle is a mechanism to correctly divide and partition within the host cell [28]. Compared to their red algal precursors, apicoplasts are surrounded by two additional membranes, the outermost of which is an endosomal membrane. During the early phase in the endosymbiotic relationship, ARC5 and FtsZ were encoded by the red algal genome and functioned in division of the two innermost membranes. A separate mechanism was required to divide the outer membranes, and our data suggest that DrpA may have been recruited for this role (possibly from an original role in the endosomal pathway). It is not clear why ARC5 and FtsZ were subsequently lost, but we speculate that the general reduction in size of the apicoplast that occurred upon loss of photosynthesis may have simplified this division process to the extent that DrpA alone was sufficient to mediate fission. It is noteworthy that DrpA homologs are present in *Cryptosporidium* species (Figure 1), Apicomplexa that are thought to have lost their apicoplast. It is conceivable that *Cryptosporidium* DrpA has acquired a novel function but equally possible that the role of DrpA in apicoplast fission evolved more recently. Examining the functions of DrpA homologs in *Cryptosporidium* and other alveolates should provide clues to how and when its role in apicoplast fission evolved.

We demonstrate that ablation of DrpA function results in specific defects in apicoplast fission. We also demonstrate a role for the extension of daughter buds in generating the U shape of apicoplasts that immediately precedes fission. Likely, this process is mediated by growth of subpellicular microtubules, and we have previously shown that treatment of *T. gondii* with the microtubule-disrupting agent oryzalin, which disrupts subpellicular microtubules, inhibits apicoplast fission [6]. Based on these observations, we have argued that the force generated by daughter budding is required for apicoplast fission [5, 6]. We now extend this model to include a role for DrpA. Although strong DrpA labeling is apparent at the site

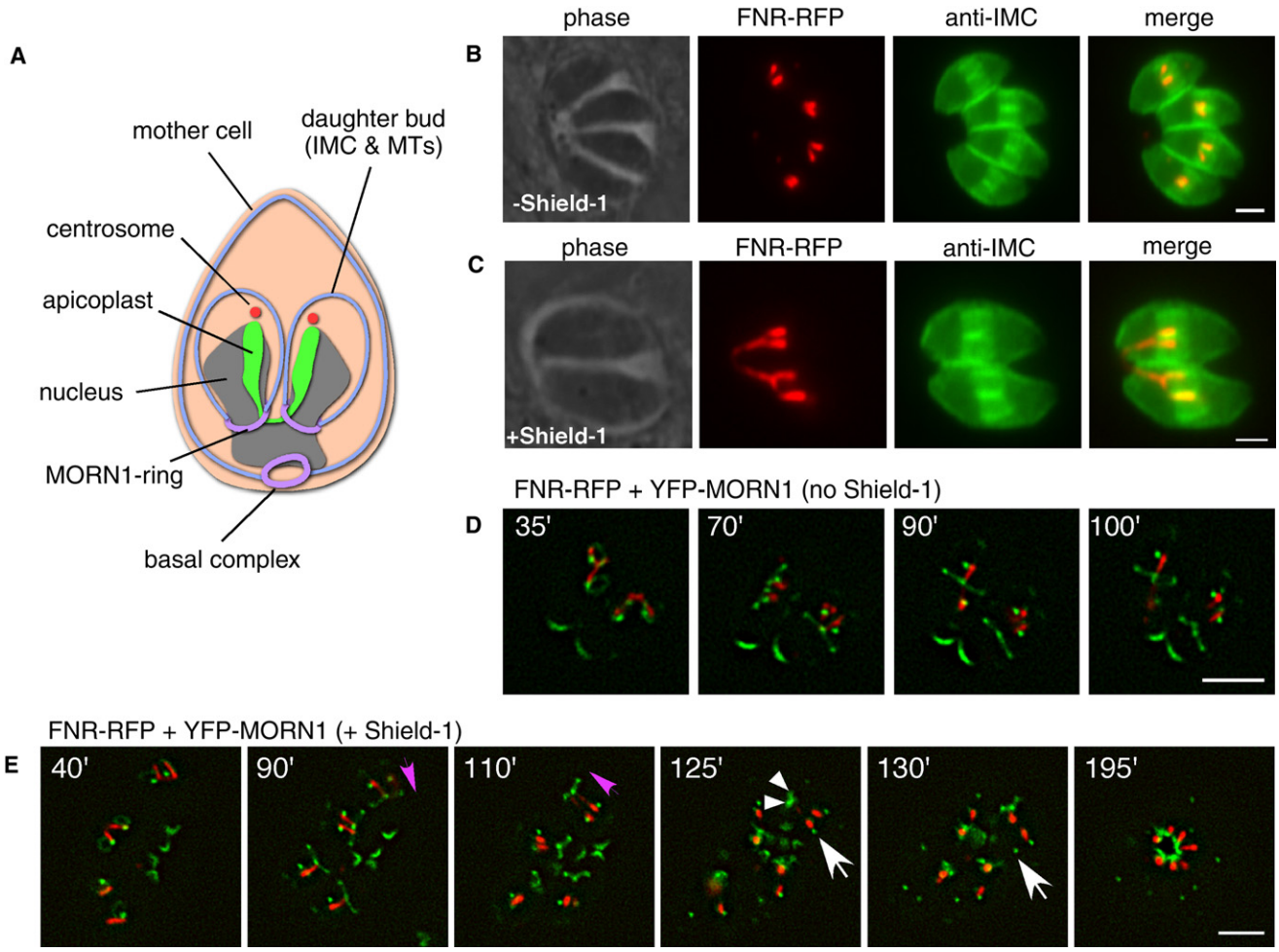

Figure 7. *Tg*DrpA Has a Direct Role in Apicoplast Fission

(A) Schematic of a dividing *T. gondii* parasite. The daughter bud (blue) comprises of subpellicular microtubules and the inner membrane complex (IMC). Subpellicular microtubules and an IMC are also present in the mother cell. MORN1 (lilac) labels the basal end of the mother cell (basal complex), the growing ends of the daughter buds (MORN1-ring), and the centrocone, an extension of the nuclear envelope that localizes near the centrosomes (red). A predivided, U-shaped apicoplast (green) and a predivided nucleus (gray) are also depicted.

(B and C) Immunofluorescence assay of DD-DrpA^{K42A} parasites grown in the absence (B) or presence (C) of Shield-1, coexpressing apicoplast RFP (red) and labeled with an anti-IMC antibody (green). The inner membrane complex of daughter cell buds can be seen inside the mother cells, with the ends of the daughter IMC localizing at the base of the dividing, U-shaped apicoplasts.

(D) Time-lapse imaging of DD-DrpA^{K42A} parasites grown in the absence of Shield-1, coexpressing FNR-RFP and YFP-MORN1. YFP-MORN1 labels the basal end of the parasites, the centrocone (an extension of the nuclear envelope that localizes adjacent to the centrosome), and the growing bud of the daughter cell.

(E) Time-lapse imaging of DD-DrpA^{K42A} parasites grown in the presence of Shield-1, coexpressing FNR-RFP and YFP-MORN1. Purple arrows in 90 and 110 min samples represent the direction of daughter cell budding. Note that, between the 90 and 110 min time points, this cell rotates almost 180°. Arrowheads at 125 min depict the MORN1-labeled basal complex, and white arrows at 125 and 130 min label a point of attachment of the apicoplast to the centrosome/centrocone that is released 5 min later. Scale bars, 2 μm.

of apicoplast fission, DrpA associates with the apicoplast at all points in the cell cycle (Figures 2A–2C). Why, then, does DrpA-mediated fission only occur during daughter cell budding? In Figure 8, we present a model for how fission and budding are mechanistically coordinated. Apicoplast ends become associated with centrosomes, which anchor them to the apical end of the cell. Soon after, daughter budding commences, with the ends of the forming daughter cells (as marked by the MORN-1 ring) stretching and, consequently, constricting the apicoplast. In yeast, dynamin-mediated mitochondrial fission requires the assembly of dynamin spirals around the organelle at the site of fission [29]. It is thought that these spirals form at sites where mitochondria are already constricted [29, 30]. A recent study of the DrpA homolog in the apicomplexan *Plasmodium falciparum* (PfDYN2) demonstrated that PfDYN2 is capable of self-association and GTP hydrolysis [31], suggesting that DrpA likely functions in a similar way to other characterized dynamin-related proteins. We propose that the stretching of U-shaped apicoplasts by forming daughter cells constricts the organelle to the extent that DrpA can assemble in spirals. As in other dynamin-based constriction models, GTP hydrolysis causes extension of the DrpA spiral (Figure 2C, arrowheads) and results in further constriction of the apicoplast until organellar fission is complete. In such a way, parasites can coordinate apicoplast fission with cytokinesis. Under this model, daughter cell budding is responsible for initial

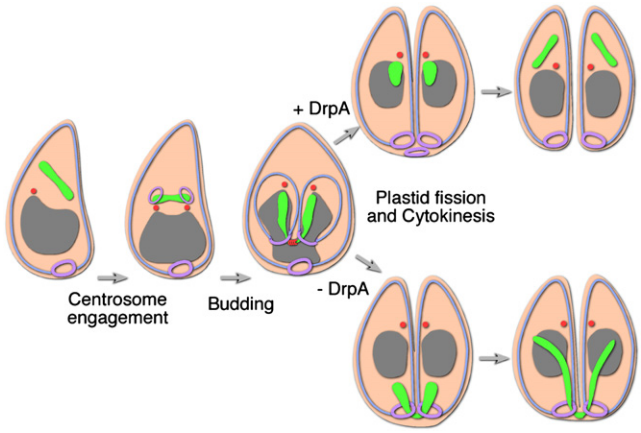

Figure 8. Model for the Role of *Tg*DrpA in Apicoplast Fission

Before daughter cell budding, centrosomes (red) anchor the apicoplast (green) to the apical end of the cell. Extension of the daughter bud (lilac) results in formation of a U-shaped apicoplast, constricting the apicoplast at the base of the U. DrpA is then able to assemble into functional, multimeric spirals (red) that hydrolyze GTP and function in the actual fission of the apicoplast. When functional DrpA is present (top right), apicoplasts divide and properly segregate with centrosomes into daughter parasites. In the absence of functional DrpA, apicoplast fission is unable to occur. Extension of the daughter bud generates the force necessary to release apicoplasts from centrosomes, with apicoplasts then localizing to the basal end of the newly formed daughter parasites (bottom right). Apicoplasts in the two newly formed daughter cells remain connected and elongate before the next round of cell division.

constriction of the apicoplast, DrpA functions in the actual fission process, and centrosome attachment mediates correct segregation of the apicoplast into daughter cells. Ongoing studies seek to experimentally test this model.

Experimental Procedures

Parasite Culture and Manipulation

Parasites were grown in human foreskin fibroblasts as previously described [32]. We grew DrpA^{K42A} mutant parasites in 0.1–0.2 μM Shield-1 (a kind gift from Tom Wandless, Stanford University) where applicable. Fluorescence growth assays were performed as previously described [20]. Cloning and plasmid construction are described in the Supplemental Data.

Phylogenetic Analyses

We generated multiple sequence alignments of dynamin homologs from a range of organisms by using ClustalX. Sequences that were used for alignments were identified on publicly available databases. Phylogenetic analyses were performed with PHYLIP as previously described [33]. The GenBank accession number for *Tg*DrpA is FJ264918. Accession numbers for other proteins used in the alignment are listed in the Supplemental Data. Alignments are available from the authors upon request.

Protein Analyses

Western blotting and pulse-chase analyses were performed as described previously [34]. For western blotting, we used anti-HA antibodies (Roche) at a dilution of 1:100 and anti-GRA8 (a kind gift from Gary Ward, University of Vermont) at 1:200,000.

Microscopy

Fluorescence and live cell images were acquired with both a DM IRBE inverted epifluorescence microscope (Leica) fitted with a 100× oil-immersion objective lens (PL APO 1.40 NA) and an IX71 inverted epifluorescence microscope (Olympus) with a 100× oil-immersion lens (UPlanApo 1.35 NA). Images on the Leica microscope were recorded with a Hamamatsu C4742-95 digital camera and adjusted for brightness and contrast with Openlab software (Improvision). Images on the Olympus microscope were recorded with a Photometrics Coolsnap HQ camera and processed with SoftWoRx software (Applied Precision). Time-lapse imaging was performed in a humidified chamber heated to 37°C with 5% CO_2, with cells grown in Mattek glass-bottom culture dishes. Images were processed to account for cell drifting. Photobleaching of RFP in the apicoplast was performed on the Olympus microscope by using ten 300 ms pulses with a 488 nm laser on a specified, diffraction-limited region. Conditions for bleaching of RFP in the mitochondrion were identical, except that we used 1 s pulses. Immunofluorescence assays were performed as previously described [34]. We used anti-ACP antibodies at a dilution of 1:2000, anti-HA at 1:50 to 1:100, anti c-*myc* (Roche) at 1:500, anti-MIC5 at 1:500, anti-ROP4 (a kind gift from Gary Ward, University of Vermont) at 1:500, and anti-IMC (Mab 45.36; a kind gift from Gary Ward, University of Vermont) at 1:500 to 1:2000. For electron microscopy, we fixed cells with 2.5% glutaraldehyde in 0.1 M phosphate buffer (pH 7.4) for 2 hr at room temperature, followed by fixation with 1% osmium tetroxide in 0.1 M cacodylate buffer (pH 7.4) for 2 hr on ice. Afterwards, the samples were brought through a graded series of ethanol and subsequently infiltrated with increasing concentrations of Epon:ethanol (3:1; 1:1; 1:3 for 2 hr each and finally pure Epon overnight). Following change for fresh Epon, samples were polymerized at 60°C for 48 hr and sectioned as monolayers. Sections (60 nm) were collected on Formvar-coated, carbon-stabilized hexagonal 100 mesh copper grids and poststained for 4 min with 20% (w/v) uranyl acetate in 70% (v/v) methanol/water followed by 2 min Reynolds's lead citrate staining [35]. The grids were examined in a transmission electron microscope Tecnai 12 (FEI Company, Eindhoven, The Netherlands) at 120 kV. Images were recorded with a CCD camera (MegaView II, Olympus Soft Imaging Solutions GmbH, Münster, Germany). Image processing was done with Analysis 3.2 (Soft Imaging Systems GmbH, Münster, Germany).

Supplemental Data

Supplemental Data include Supplemental Experimental Procedures, four figures, and five movies and can be found with this article online at http://www.current-biology.com/supplemental/S0960-9822(09)00541-7.

Acknowledgments

We thank Tom Wandless (Stanford University) for donating Shield-1, Vern Carruthers (University of Michigan), Gary Ward (University of Vermont), Jianmin Fang and Sylvia Moreno (University of Georgia), Eric Gershwin (University of California, Davis), and Geoff McFadden (University of Melbourne) for sharing antibodies and Michael White (Montana State University), Cynthia He (National University of Singapore), and Chris Tonkin (Walter and Eliza Hall Institute) for sharing plasmids. We are grateful to Sylvia Moreno and Roberto Docampo (University of Georgia) for use of their microscope, the students of the Biology of Parasitism (Woods Hole, MA) courses in 2007 and 2008 for their enthusiasm and ideas in generating preliminary data for this project, and Julie Nelson of the Center for Tropical and Emerging Global Diseases (CTEGD) Flow Cytometry Facility for performing cell sorting. This work was supported by a C.J. Martin Overseas Fellowship (400489) from the Australian National Health and Medical Research Council to G.G.v.D.; a University of Georgia Presidential Graduate Fellowship to S.B.R.; funding from the European Network of Excellence "Three-Dimensional Electron Microscopy," FP6, and the Dutch Cyttron consortium to C.T. and B.M.H.; a grant from the "BioFuture-Programm" (0311897) of the German Ministry of Science and Education (BMBF) to M.M.; and a grant from the National Institutes of Health to B.S. (AI 64671).

Received: September 18, 2008
Revised: November 18, 2008
Accepted: December 22, 2008
Published online: February 12, 2009

References

1. Beech, P.L., and Gilson, P.R. (2000). FtsZ and organelle division in Protists. Protist *151*, 11–16.
2. Gao, H., Kadirjan-Kalbach, D., Froehlich, J.E., and Osteryoung, K.W. (2003). ARC5, a cytosolic dynamin-like protein from plants, is part of the chloroplast division machinery. Proc. Natl. Acad. Sci. USA *100*, 4328–4333.
3. Miyagishima, S.Y., Nishida, K., Mori, T., Matsuzaki, M., Higashiyama, T., Kuroiwa, H., and Kuroiwa, T. (2003). A plant-specific dynamin-related

protein forms a ring at the chloroplast division site. Plant Cell *15*, 655–665.

4. He, C.Y., Shaw, M.K., Pletcher, C.H., Striepen, B., Tilney, L.G., and Roos, D.S. (2001). A plastid segregation defect in the protozoan parasite *Toxoplasma gondii*. EMBO J. *20*, 330–339.
5. Vaishnava, S., and Striepen, B. (2006). The cell biology of secondary endosymbiosis—How parasites build, divide and segregate the apicoplast. Mol. Microbiol. *61*, 1380–1387.
6. Striepen, B., Crawford, M.J., Shaw, M.K., Tilney, L.G., Seeber, F., and Roos, D.S. (2000). The plastid of *Toxoplasma gondii* is divided by association with the centrosomes. J. Cell Biol. *151*, 1423–1434.
7. Vaishnava, S., Morrison, D.P., Gaji, R.Y., Murray, J.M., Entzeroth, R., Howe, D.K., and Striepen, B. (2005). Plastid segregation and cell division in the apicomplexan parasite *Sarcocystis neurona*. J. Cell Sci. *118*, 3397–3407.
8. Striepen, B., Jordan, C.N., Reiff, S., and van Dooren, G.G. (2007). Building the perfect parasite: Cell division in apicomplexa. PLoS Pathog. *3*, e78.
9. Ferguson, D.J., Henriquez, F.L., Kirisits, M.J., Muench, S.P., Prigge, S.T., Rice, D.W., Roberts, C.W., and McLeod, R.L. (2005). Maternal inheritance and stage-specific variation of the apicoplast in *Toxoplasma gondii* during development in the intermediate and definitive host. Eukaryot. Cell *4*, 814–826.
10. Matsuzaki, M., Kikuchi, T., Kita, K., Kojima, S., and Kuroiwa, T. (2001). Large amounts of apicoplast nucleoid DNA and its segregation in *Toxoplasma gondii*. Protoplasma *218*, 180–191.
11. Praefcke, G.J., and McMahon, H.T. (2004). The dynamin superfamily: Universal membrane tubulation and fission molecules? Nat. Rev. Mol. Cell Biol. *5*, 133–147.
12. Miyagishima, S.Y., Kuwayama, H., Urushihara, H., and Nakanishi, H. (2008). Evolutionary linkage between eukaryotic cytokinesis and chloroplast division by dynamin proteins. Proc. Natl. Acad. Sci. USA *105*, 15202–15207.
13. Rahaman, A., Elde, N.C., and Turkewitz, A.P. (2008). A dynamin-related protein required for nuclear remodeling in *Tetrahymena*. Curr. Biol. *18*, 1227–1233.
14. Elde, N.C., Morgan, G., Winey, M., Sperling, L., and Turkewitz, A.P. (2005). Elucidation of clathrin-mediated endocytosis in *Tetrahymena* reveals an evolutionarily convergent recruitment of dynamin. PLoS Genet. *1*, e52.
15. Breinich, M.S., Ferguson, D.J.P., Foth, B.J., van Dooren, G.G., Lebrun, M., Quon, D.V., Striepen, B., Bradley, P.J., Frischknecht, F., Carruthers, V.B., et al. (2009). A dynamin is required for the biogenesis of secretory organelles in Toxoplasma gondii. Curr. Biol. *19*, this issue, 277–286.
16. van der Bliek, A.M., Redelmeier, T.E., Damke, H., Tisdale, E.J., Meyerowitz, E.M., and Schmid, S.L. (1993). Mutations in human dynamin block an intermediate stage in coated vesicle formation. J. Cell Biol. *122*, 553–563.
17. Otsuga, D., Keegan, B.R., Brisch, E., Thatcher, J.W., Hermann, G.J., Bleazard, W., and Shaw, J.M. (1998). The dynamin-related GTPase, Dnm1p, controls mitochondrial morphology in yeast. J. Cell Biol. *143*, 333–349.
18. Banaszynski, L.A., Chen, L.C., Maynard-Smith, L.A., Ooi, A.G., and Wandless, T.J. (2006). A rapid, reversible, and tunable method to regulate protein function in living cells using synthetic small molecules. Cell *126*, 995–1004.
19. Herm-Gotz, A., Agop-Nersesian, C., Munter, S., Grimley, J.S., Wandless, T.J., Frischknecht, F., and Meissner, M. (2007). Rapid control of protein level in the apicomplexan *Toxoplasma gondii*. Nat. Methods *4*, 1003–1005.
20. Gubbels, M.J., Li, C., and Striepen, B. (2003). High-throughput growth assay for *Toxoplasma gondii* using yellow fluorescent protein. Antimicrob. Agents Chemother. *47*, 309–316.
21. Fichera, M.E., and Roos, D.S. (1997). A plastid organelle as a drug target in apicomplexan parasites. Nature *390*, 407–409.
22. Gubbels, M.J., Vaishnava, S., Boot, N., Dubremetz, J.F., and Striepen, B. (2006). A MORN-repeat protein is a dynamic component of the *Toxoplasma gondii* cell division apparatus. J. Cell Sci. *119*, 2236–2245.
23. Hu, K. (2008). Organizational changes of the daughter basal complex during the parasite replication of *Toxoplasma gondii*. PLoS Pathog. *4*, e10.
24. Nishi, M., Hu, K., Murray, J.M., and Roos, D.S. (2008). Organellar dynamics during the cell cycle of *Toxoplasma gondii*. J. Cell Sci. *121*, 1559–1568.
25. Hu, K., Johnson, J., Florens, L., Fraunholz, M., Suravajjala, S., DiLullo, C., Yates, J., Roos, D.S., and Murray, J.M. (2006). Cytoskeletal components of an invasion machine–the apical complex of *Toxoplasma gondii*. PLoS Pathog. *2*, e13.
26. Moore, R.B., Obornik, M., Janouskovec, J., Chrudimsky, T., Vancova, M., Green, D.H., Wright, S.W., Davies, N.W., Bolch, C.J., Heimann, K., et al. (2008). A photosynthetic alveolate closely related to apicomplexan parasites. Nature *451*, 959–963.
27. Fast, N.M., Kissinger, J.C., Roos, D.S., and Keeling, P.J. (2001). Nuclear-encoded, plastid-targeted genes suggest a single common origin for apicomplexan and dinoflagellate plastids. Mol. Biol. Evol. *18*, 418–426.
28. Okamoto, N., and Inouye, I. (2005). A secondary symbiosis in progress? Science *310*, 287.
29. Ingerman, E., Perkins, E.M., Marino, M., Mears, J.A., McCaffery, J.M., Hinshaw, J.E., and Nunnari, J. (2005). Dnm1 forms spirals that are structurally tailored to fit mitochondria. J. Cell Biol. *170*, 1021–1027.
30. Legesse-Miller, A., Massol, R.H., and Kirchhausen, T. (2003). Constriction and Dnm1p recruitment are distinct processes in mitochondrial fission. Mol. Biol. Cell *14*, 1953–1963.
31. Charneau, S., Bastos, I.M., Mouray, E., Ribeiro, B.M., Santana, J.M., Grellier, P., and Florent, I. (2007). Characterization of PfDYN2, a dynamin-like protein of *Plasmodium falciparum* expressed in schizonts. Microbes Infect. *9*, 797–805.
32. Striepen, B., and Soldati, D. (2007). Genetic manipulation of *Toxoplasma gondii*. In *Toxoplasma gondii.* The Model Apicomplexan—Perspectives and Methods, L.D. Weiss and K. Kim, eds. (London: Elsevier), pp. 391–415.
33. Foth, B.J. (2007). Phylogenetic analysis to uncover organellar origins of nuclear-encoded genes. Methods Mol. Biol. *390*, 467–488.
34. van Dooren, G.G., Tomova, C., Agrawal, S., Humbel, B.M., and Striepen, B. (2008). *Toxoplasma gondii* Tic20 is essential for apicoplast protein import. Proc. Natl. Acad. Sci. USA *105*, 13574–13579.
35. Reynolds, E.S. (1963). The use of lead citrate at high pH as an electron-opaque stain in electron microscopy. J. Cell Biol. *17*, 208–212.